On the driving factors of the future changes in the wintertime Northern-Hemisphere atmospheric waviness

A. Yamamoto[1] and P. Martineau[2]

[1]J. F. Oberlin University, Machida, Tokyo, Japan
[2]Japan Agency for Marine-Earth Science and Technology, Yokohama, Kanagawa, Japan

Key Points:

- Biases in Northern Hemisphere wintertime climatological waviness in historical runs are mostly ameliorated with high-resolution models
- Future Northern Hemisphere winter waviness will undergo a general reduction, which is mitigate by high-resolution models over North Atlantic
- Sensible heat fluxes play a crucial role in both historical biases and future reductions in waviness, highlighting the key role of the ocean

Corresponding author: Ayako Yamamoto, `yamamoto_a@obirin.ac.jp`

Abstract

Despite the significant socioeconomic implications in the link between atmospheric waviness and extreme weather events, future atmospheric waviness trends remain elusive due to uncertainties arising from diverse definitions and insufficient dynamical formalism in existing metrics. This study employs a local wave activity (LWA) metric, whose prognostic equation links wave activity changes to forcing mechanisms, to assess wintertime Northern Hemisphere waviness in ERA5 and HighResMIP datasets. The models generally exhibit high fidelity in reproducing observed waviness, while biases stem primarily from biases in the LWA source, low-level meridional heat flux, which tend to improve with higher resolutions. Future projections exhibit reduction in LWA, primarily due to suppressed LWA generation, which is mitigated by higher-resolution models. We found that both biases and reduction of the LWA source are closely associated with sensible heat fluxes from the ocean to the atmosphere, highlighting the potential impacts of resolving ocean currents.

1 Introduction

In the mid-latitude atmosphere, surface weather is tightly coupled with fluctuations of the circulation aloft that is associated with the propagation of atmospheric waves. These atmospheric waves in turn are closely linked to the frequency and severity of extreme weather events (Martineau et al., 2017). As such, there has been a growing interest in the past decade to characterize and understand changes in waviness of the midlatitude circulation.

Based on a metric quantifying the meandering of arbitrary geopotential height contours, Francis and Vavrus (2012) proposed that waviness of the extratropical Northern Hemisphere (NH) circulation had been amplifying as a consequence of Arctic amplification, the escalated near-surface warming over the Arctic. Barnes (2013), however, challenged this claim, suggesting that the positive trend found in their study may be an artefact of the metric used. Using an improved metric, also based on geopotential height, she revealed a lack of robust waviness trends in the historical record. Henceforth, many studies have assessed waviness trends based on the meridional excursion of contours of different variables such as potential vorticity (PV) (Röthlisberger et al., 2016) and geopotential height (Cattiaux et al., 2016; Di Capua & Coumou, 2016; Martin, 2021), or the amplitude of circulation anomalies with respect to the zonal mean (Coumou et al., 2015). It is, however, generally challenging to draw a unanimous conclusion on the observed and future trends of waviness from these diverse metrics (Geen et al., 2023; Nie et al., 2023).

Notably, Screen and Simmonds (2013) highlighted the sensitivity of waviness trend assessments to the consideration of waves as meandering of contours or zonal anomalies. Chen et al. (2015) and Martineau et al. (2017) sought to reconcile these two concepts by using a metric factoring in both meridional displacements of geopotential height contours and amplitude of the enclosed anomalies. This new metric, together with the predecessors, however, lack a foundation in a dynamical formalism. As such, no prognostic equation links changes in these waviness metrics to forcing mechanisms.

A waviness metric called local wave activity (LWA) developed by Huang and Nakamura (2016) overcomes this drawback, thereby possibly enhancing our comprehension in waviness trends. LWA is a conservative quantity for quasigeostrophic flows, whose governing equation links LWA time tendencies to dynamical processes. Generalizing the linear, small-amplitude theory to eddies of arbitrary amplitude, LWA has demonstrated its usefulness in capturing extreme jet meandering events such as atmospheric blocking, while enabling the diagnosis of physical processes that drive waviness (Huang & Nakamura, 2016; Nakamura & Huang, 2018; Neal et al., 2022; Wang et al., 2021).

Here, we employ the LWA budget analysis to assess historical and future waviness. In view of a growing body of evidence that enhancing model resolution improves the representation of transient eddies (Boville, 1991) and large-scale atmospheric variability (Davini & D'Andrea, 2020; Athanasiadis et al., 2022), here we apply LWA metric to a suite of low- and high-resolution climate models and a reanalysis dataset. Our study aims to 1) evaluate the fidelity of state-of-the-art climate models in reproducing waviness in the current climate, 2) diagnose waviness trends in the future climate, and 3) investigate benefits of using high-resolution models.

2 Dataset Used

We utilize selected model output from the High Resolution Model Intercomparison Project (HighResMIP; Haarsma et al., 2016). HighResMIP is a coordinated effort to systematically assess robust advantages of increasing horizontal resolution in models, given that simulation of a multitude of atmospheric and oceanic phenomena have been reported to improve with higher horizontal model resolution (see reviews in Haarsma et al., 2016). Here, "high-resolution" denotes a resolution higher than 50 km or 0.25° for the atmosphere and the ocean respectively.

We use coupled model runs from five sets of HighResMIP models (Table S1), each of which meets the following criteria: A model 1) has both low- and high-resolution versions, 2) has daily three-dimensional zonal and meridional wind speeds and temperature, and 3) has all the meteorological fields extrapolated under the topography. The latter two criteria are necessitated for the LWA computation. Table S1 illustrates that the range of high and low resolutions depends entirely on the model being used. Here, regardless of the actual model resolution, we categorize lower- and higher-resolution version of each model set as "low-resolution" and "high-resolution" model. In addition to the aforementioned three-dimensional variables that are provided on eight common pressure levels (1000, 850, 700, 500, 250, 100, 50, and 10 hPa), we use monthly-mean sensible heat fluxes (SHF) data. Here, we analyze boreal winter (December-January-February; DJF) seasons for years 1960–1995 from historical runs, and years 2015–2050 from the future runs. Since ECMWF-IFS models only provide historical runs, they are only used for the model fidelity assessment and the historical LWA budget analysis. We use one ensemble member from each model, and each dataset is interpolated onto $2° \times 2°$ horizontal grid prior to analysis.

Additionally, the fifth-generation atmospheric reanalysis dataset from European Centre for Medium-Range Weather Forecasts (ERA5; Hersbach et al., 2020) is used as a reference atmospheric dataset for the historical period. ERA5 data are interpolated on the same common grid and temporal resolution as HighResMIP prior to the analyses.

3 Local Wave Activity (LWA) diagnosis

In this study, we use local wave activity (LWA; Huang & Nakamura, 2016) as a measure of waviness. LWA is a generalization of the finite amplitude wave activity that quantifies wave activity in the pressure-latitude plane (Nakamura & Solomon, 2010) to its three-dimensional representation. The LWA quantifies waviness based on the meridional displacements of the quasi-geostrophic potential vorticity (QGPV) isolines. It is advantageous over classical definitions of eddies by its ability to quantify and provide a conservation relation that holds for eddies of finite (as opposed to small) amplitude.

LWA (A) quantified at each longitude (λ), latitude (ϕ), height (z), and time (t) is defined as follows:

$$A(\lambda, \phi, z, t) = -\frac{a}{cos\phi} \int_0^{\Delta\phi} q_e(\lambda, \phi, \phi', z, t) cos(\phi + \phi') d\phi' \qquad (1)$$

where a is the planetary radius, $\Delta\phi$ is the latitudinal displacement of a reference q contour (q_{ref}) from a zonally symmetric reference state, from which a QGPV anomaly (q_e) is defined as:

$$q_e(\lambda, \phi, \phi', z, t) = q(\lambda, \phi + \phi', z, t) - q_{ref}(\phi, z, t). \tag{2}$$

q_{ref} is computed by zonalizing the QGPV contours while preserving the enclosed areas (Nakamura & Solomon, 2010). In this formulation LWA is by definition a positive definite quantity, regardless of whether the zonal flow is perturbed by troughs or ridges (Huang & Nakamura, 2016).

When averaged over a season, LWA comprises both stationary and transient eddy components, whose straightforward partitioning is hindered partly because a reference state (Equation 2) is based on the Lagrangian average of QGPV. Here, following Huang and Nakamura (2017), we estimate the stationary component using the temporal mean of QGPV, and the transient component as the difference between total LWA and the stationary component.

The time tendency of the density-weighted vertical average (denoted by $\langle\cdots\rangle$) of LWA is defined as follows:

$$\frac{\partial}{\partial t}\langle A\rangle\cos\phi = \underbrace{-\frac{1}{a\cos\phi}\frac{\partial\langle F_\lambda\rangle}{\partial\lambda}}_{(i)\text{ zonal advective flux convergence}} + \underbrace{\frac{1}{a\cos\phi}\frac{\partial}{\partial\phi}\langle u_e v_e \cos^2(\phi)\rangle}_{(ii)\text{ eddy momentum flux divergence}} + \underbrace{\frac{f\cos\phi}{H}\left(\frac{v_e\theta_e}{\partial\tilde\theta/\partial z}\right)_{z=0}}_{(iii)\text{ low-level meridional heat flux}} + \underbrace{\langle\dot A\rangle\cos\phi}_{(iv)\text{ residual}},$$

$$\tag{3}$$

where u_e, v_e, and θ_e represent anomalies of zonal and meridional wind, as well as potential temperature, relative to their respective reference states. The terms (i) and (ii) represent zonal and meridional LWA flux convergence, respectively, whereas the term (iii) represents vertical LWA flux at the lower boundary. The term (iv) denotes residual, which results from non-quasigeostrophic processes, including diabatic processes such as vertical transport of low PV air from the lower troposphere fuelled by latent heat release (Grams & Archambault, 2016; Pfahl et al., 2015; Yamamoto et al., 2021; Neal et al., 2022).

The zonal LWA flux $\langle F_\lambda\rangle$ in term (i) is composed of three terms:

$$\langle F_\lambda\rangle = \underbrace{\langle u_{ref} A\cos\phi\rangle}_{(a)} + \underbrace{a\left\langle\int_0^{\Delta\phi} u_e q_e \cos(\phi+\phi')d\phi'\right\rangle}_{(b)} + \underbrace{\frac{\cos\phi}{2}\left\langle v_e^2 - u_e^2 - \frac{R}{H}\frac{e^{-\frac{\kappa z}{H}}}{\partial\tilde\theta/\partial z}\theta_e^2\right\rangle}_{(c)}, \tag{4}$$

where terms (a) and (b) make up of advective LWA flux. Here, we investigate these density-weighted vertical averages, given the quasi-barotropic nature of these phenomena.

4 LWA Biases in Historical Runs

Comparison of the climatological wintertime LWA spatial distribution in the historical period for ERA5 and the multi-model mean (MMM) of all the HighResMIP models used (top two panels of Figure 1a) reveals that the general features in ERA5 are well captured by MMM, including the two distinct maxima observed over the Pacific and Atlantic sectors. This spatial distribution resembles that of wintertime climatological-mean frequency of blocking, an atmospheric phenomenon that disturbs the jet stream path and consequently affects waviness (see Figure 2 of Woollings et al., 2018).

The MMM bias of LWA against ERA5 in the historical record (Figure 1a lower-left panel) illustrates that waviness maximum found over Europe is underestimated by the models by approximately 10%, which is also fairly analogous to the well-known common model bias for the European blocking frequencies. This model bias stems from a lack of anticyclonic wave breaking and bias in the eddy-driven jet, which, while alleviated compared to the predecessors, are still prevalent in CMIP6 models (Davini & D'Andrea, 2020; Athanasiadis et al., 2022). Thus, the negative LWA bias also likely reflects these biases in models. Decomposition of the observed and the MMM LWA into its stationary and transient components (Figure S1) reveals that this negative bias stems solely from the stationary component, hinting that underestimation in blocking frequency has an imprint on the suppressed time-mean ridge. Conversely, the MMM LWA over much of the mid-latitude Pacific and Eurasia overestimates the observed waviness strength. While the excessive LWA over the Pacific stems from both stationary and transient components, it mostly originates from the transient component over Eurasia (Figure S1). These sectors where the MMM LWA positive biases are found correspond to where the vertically-averaged MMM zonal wind exhibits negative biases against ERA5, suggesting that a wavier flow is accompanied by a reduction in zonal winds (Figure S2). The difference in model bias between high-resolution and low-resolution models (Figure 1a lower-right panel) shows that biases in the high-resolution models are generally reduced over eastern Eurasia and southwestern edge of Atlantic, though slightly amplified in the vicinity of Iceland.

The reproducibility of the LWA spatial pattern in the historical record by each model is shown in a Taylor diagram (Figure 1b). It is evident that each model simulates the climatological LWA pattern fairly well, which typically improves with high-resolution models (up-pointing triangles) compared to their low-resolution counterparts (down-pointing triangles), while the extent of improvement highly depends on the model. HiRAM-SIT-HR is an exception, which, despite having a high correlation, displays much lower standard deviation compared to HiRAM-SIT-LR. As shown in Figure S3, HiRAM-SIT-HR shows a weaker climatological LWA compared to ERA5, particularly over the North Atlantic sector. As whether including this model or not did not qualitatively change the results for the rest of the analyses, we retain this model in the rest of our analysis.

5 LWA budget analyses in the historical period

Figure 2 illustrates the climatology of the first three terms in the LWA tendency equation (Equation 3), demonstrating the LWA budget. It is evident that for both ERA5 and MMM, low-level meridional heat flux (Figure 2c) acts as a LWA source over both the Atlantic and Pacific sectors (encircled by black contours) as well as over the Gulf of Alaska, indicated by the positive (i.e., poleward) signal, consistent with Huang and Nakamura (2017). While the LWA source maxima over the Pacific and the Gulf of Alaska are locally confined, the LWA source over the Atlantic sector spans further to the northeast following the North Atlantic Current, an extension of the warm Gulf Stream. Huang and Nakamura (2017) attributed a significant portion of this elongated signal to the quasi-stationary zonal asymmetry in low-level potential temperature which arises from the underlying sea surface temperature (SST) distribution and the accompanying meridional wind. This LWA production is largely compensated by the zonal advective flux divergence (Figure 2a), such that LWA is redistributed mainly downstream. The eddy momentum flux divergence (Figure 2b) also acts as a sink, though to a much lesser extent.

When compared to ERA5, models tend to underestimate the low-level meridional heat flux upstream of the Atlantic LWA maximum (Figure 2 third column). This suppressed LWA source appears to stem from the subdued SHF from the ocean to the atmosphere in the vicinity of so-called Northwest Corner, the beginning of the North Atlantic Current (Figure 2d). This region coincides with where a strong cold SST bias is commonly found in the ocean-sea-ice simulations (Tsujino et al., 2020), which gives rise to the negative SHF bias. Together with the overestimation of SHF over the North At-

lantic south of Iceland, these SHF biases lead to the subdued meridional heat flux, causing the suppressed LWA source over this region. Consequently, the downstream LWA redistribution by zonal advective flux divergence is weaker than ERA5 (i.e., positive bias), resulting in the LWA underestimation over the Atlantic sector. This result is consistent with Athanasiadis et al. (2022), who showed that the reduced cold SST bias at the Northwest Corner generally leads to improved representation of European blocking in climate models, due to the ameliorated low-level baroclinicity.

On the contrary, overestimation of the MMM LWA over much of the rest of the NH midlatitudes stems from excessive LWA production by low-level meridional heat flux over the eastern edge of Eurasian continent and the vicinity of the Gulf of Alaska (Figure 2c), which results in extra LWA advection downstream over both of these regions (Figure 2a). The excessive LWA sources are mostly attributable to positive SHF bias over Japan Sea and off the west coast of North America (Figure 2d), while the positive bias in LWA source on the western flank of the Pacific likely stems from the anomalously large southward negative heat flux (Figure S4f).

The last column of Figure 2 illustrates that higher resolution models systematically reduce the suppressed low-level meridional heat flux bias over the western edge of the Atlantic LWA maximum and eastern edge of the Eurasia, leading to the improved model fidelity in LWA. This better model fidelity should also be ascribable to the ameliorated SHF over both of these regions (Figure 2d).

6 Historical vs. future LWA

The future LWA projection features a general LWA reduction, particularly at the southern flanks of maxima over the Atlantic and Pacific sectors and over the Gulf of Alaska (Figure 3a third column), which are all mostly attributable to the stationary component (Figure S5). Reduction over the northern flanks of the Atlantic LWA maximum is mitigated with high-resolution models compared to the low-resolution counterparts (Figure 3a fourth column), which is also solely due to the stationary component (Figure S5). An exception for this general reduction in waviness is found near Barents-Kara Sea, where over three-quarters of models investigated suggest future waviness increase. This region coincides with where a statistically significant positive LWA trend is found in the historical period (Nakamura & Huang, 2018, see their Figure S6).

The LWA budget retains its balance in the future projection, such that the low-level meridional heat flux acts as the primary LWA source (Figure 3d), while zonal advective flux divergence (Figure 3b) acts as the primary sink over both the Atlantic and Pacific sectors and over the Gulf of Alaska, redistributing LWA downstream. This LWA source is projected to decrease in the future particularly in the north of Iceland and Japan, which results in reduced LWA downstream redistribution by zonal advective flux divergence (i.e., increase in convergence) and LWA reduction. We found that these areas coincide with reduced SHF transfer from the ocean to the atmosphere in the extratropics, while closer to the pole, SHF release to the atmosphere increases, due likely to the future sea ice melting (Figure 3e). These contrasting SHF changes in turn result in the reduced meridional heat flux. Intriguingly, this future reduction in both LWA source and sink is damped in the majority of high-resolution models, inducing less projected LWA reduction. Figure 3e further reveals a strong positive signal over the Kuroshio extension and weak but significant positive signal over the North Atlantic Current in SHF of high-resolution models, indicating that suppression in the LWA reduction is attributable to resolving larger ocean heat fluxes released from the western boundary currents. The waviness increase found near Barents-Kara Sea, in contrast, is characterized by amplified divergence of zonal advective flux, without any increase in LWA source by low-level meridional heat flux (Figure S6), possibly indicating an enhanced waviness due to diabatic sources.

Figure 4a summarizes the contribution by each term comprised in the LWA time tendency equation (Equation 3) along with the residual term obtained by assuming the tendency to become zero climatologically, over the Pacific Sector (encircled area on Figures 2 and 3). It is evident that (iii) low-level meridional heat flux stands alone as the primary LWA source over the Pacific sector for both ERA5 and models. For ERA5, the LWA production is balanced by (i) zonal advective flux divergence (73.2%), (ii) eddy momentum flux divergence (16.7%), and (iv) residual (10.1%). For the low-resolution models in historical run, LWA production is overestimated by 12.4% compared to ERA5 on average, which is reduced to 3.4% with high-resolution counterparts. LWA production in the future decreases compared to the historical run by 6.9% and 6.7% for low- and high-resolution models, respectively.

Figure 4b summarizes the balance of each term over the Atlantic Sector. In contrast to the Pacific, it is apparent that (iv) residual acts as a secondary LWA source, along with (iii) low-level meridional heat flux. This is consistent with the fact that this Atlantic Sector coincides with the outflow region of a large-scale cross-isentropic ascent associated with extratropical cyclones called a warm conveyor belt (WCB; Madonna et al., 2014), which can increase the upper-level waviness by bringing low-PV air from the lower troposphere (Grams & Archambault, 2016; Pfahl et al., 2015; Yamamoto et al., 2021). For ERA5, (iii) low-level meridional heat flux explains 62.6% of the LWA production, whereas the rest is due to (iv) residual. 90.9% of this LWA production is redistributed by (i) zonal advective flux divergence. Underestimation of the LWA source with low- and high-resolution models compared to ERA5 amount to 11.4% and 12.9%, respectively, while excluding HiRAM-SIT models enhances agreement with ERA5 for high-resolution models (Figure S7). In the future, LWA production decreases compared to the historical run, by 16.1% and by 11.9% for low-resolution and high-resolution models, respectively, which is primarily balanced by the decrease in (i) zonal advective flux convergence for both sets of models.

7 Conclusion and Discussion

In this study, by applying a local wave activity (LWA) analysis to both a suite of low- and high-resolution climate models and a reanalysis dataset, we characterized the historical model bias and future changes in the Northern Hemisphere wintertime climatological waviness, and identified causes behind them.

We found that both the biases in the historical LWA source and the reduction in the future LWA source are associated with biases and reductions in sensible heat flux (SHF) over the oceans, respectively. High-resolution models better resolve SHF and suppresses both biases and reduction of LWA, thus pointing towards the importance of having higher ocean resolution for an accurate future waviness projection. In the present study we have highlighted the potential role of the ocean for the atmospheric waviness from a climatological perspective. Understanding how sensitive waviness is to oceanic variabilities on shorter time scales also has important implications.

Additionally, the analysis illustrated that the residual term serves as a LWA source over the Atlantic on average, which undergoes reduction in the future. This result appears to suggest a projected reduction in fuelling low potential-vorticity air from low latitude and low altitude via warm conveyor belt (WCB) over the region (Grams & Archambault, 2016; Pfahl et al., 2015; Yamamoto et al., 2021). This assumption, however, is in apparent odds with a recent study which found a general increase in the WCB intensity in a future simulation (Joos et al., 2023). A quantitative assessment of how much this vertically-transported low potential-vorticity air sets waviness in the changing climate remains to be conducted.
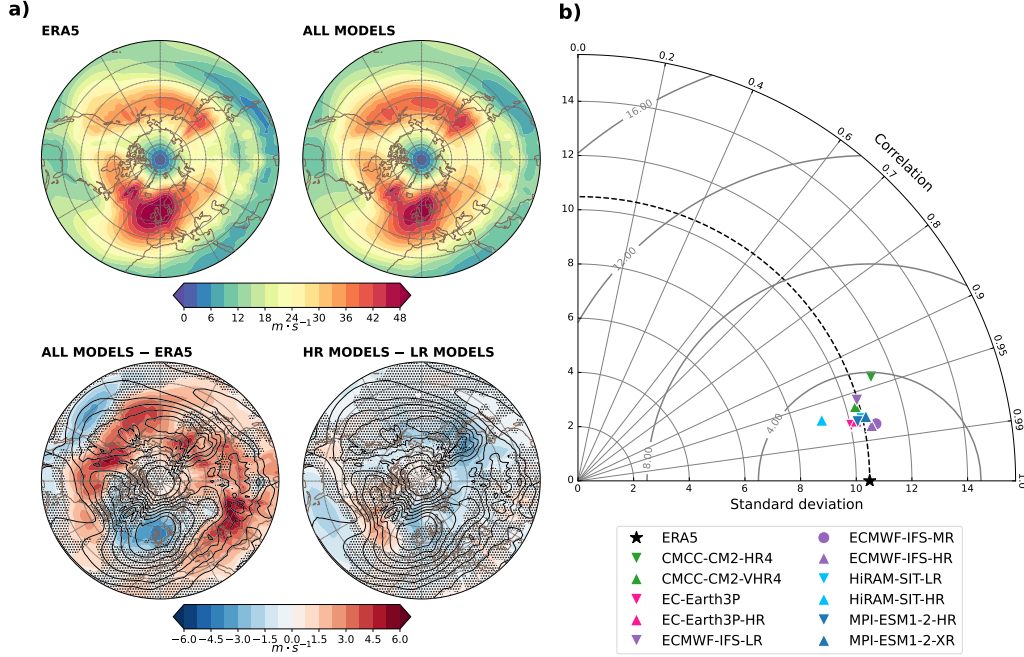
Figure 1. a) DJF LWA climatology [m s^{-1}] computed using ERA5 (top left) and all High-ResMIP models (top right), the difference in the LWA climatology between all HighResMIP models and ERA5 (bottom left), and the difference between high-resolution (HR) and low-resolution (LR) models (bottom right). The unstippled areas in the last bottom two panels indicate where a sign of the mean difference agrees with at least three-quarters of models, and black contours indicate the ERA5 DJF LWA climatology. b) Taylor diagram displaying a statistical comparison of LWA computed with HighResMIP models and ERA5.

8 Open Research Statement

All HighResMIP model output (Haarsma et al., 2016) are publicly available at ESGF (`https://esgf.llnl.gov/`). The ERA5 dataset (Hersbach et al., 2020) is available at CDS (`https://cds.climate.copernicus.eu`) platform. LWA was computed using the Python Library falwa v1.2.1 (Huang, 2024).
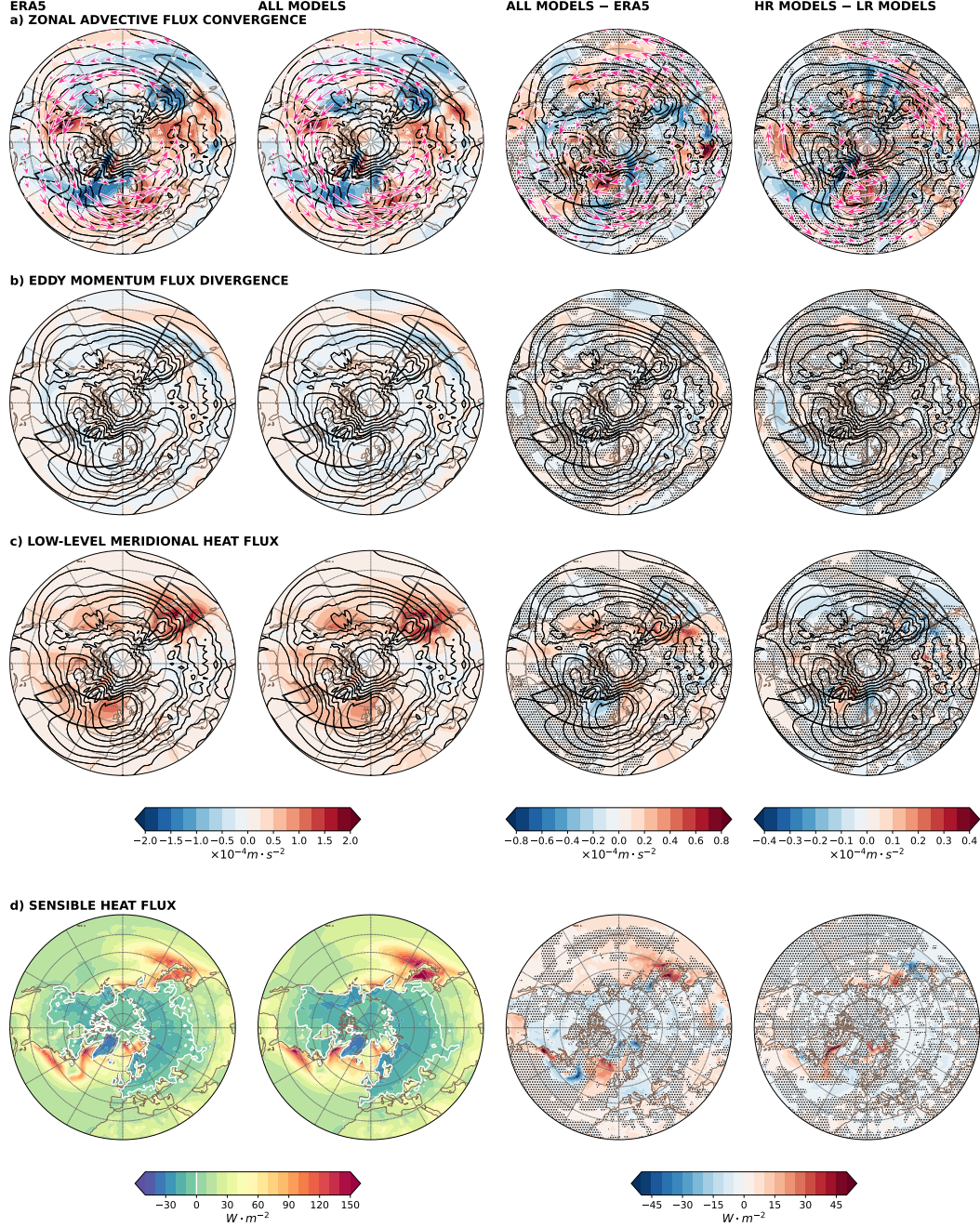
Figure 2. Historical DJF climatology of the first three terms in the LWA time tendency equation (Equation 3): a) Zonal advective flux convergence (shade) and the zonal LWA flux (arrows), b) eddy momentum flux divergence, c) low-level meridional heat flux, and d) SHF (positive upward). For panels a) – c), black contours indicate the ERA5 LWA DJF climatology and black thick lines encircle the areas investigated in Figure 4 (Pacific: a rectangle bounded by $[30°N–60°N]×[120°E–150°E]$, Atlantic: a parallelogram bounded by $[30°N–50°N]$ at $70°W$ and $[50°N–70°N]$ at $0°$). Each column denotes results with ERA5 (left column), HighResMIP models (second column), the difference between all models and ERA5 (third column), and the difference between high-resolution and low-resolution models (last column). The unstippled areas in the last two columns indicate where a sign of the mean difference agrees with at least three-quarters of models.
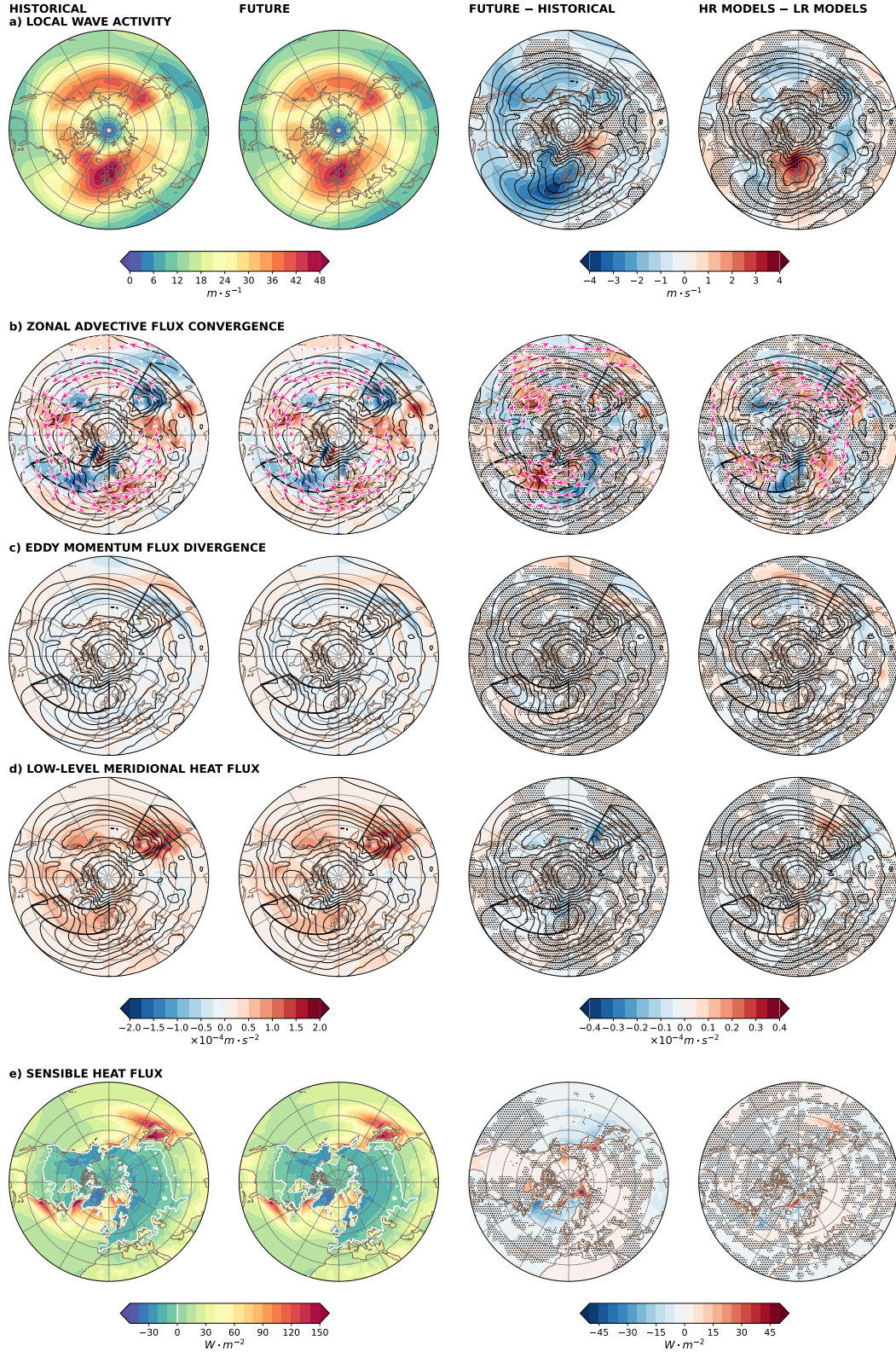
Figure 3. a) Same as Figure 1a, but for the DJF climatology of historical (first column) and future (second column) simulations. b) – e) Same as Figure 2 but for the DJF climatology of historical (first column) and future (second column) simulations. (Third column) the difference between future and historical climatology and (fourth column) the difference between future and historical climatology for high-resolution models minus that for low-resolution models of the respective fields. Black contours for panels a) – d) indicate the historical LWA DJF climatology of all models.
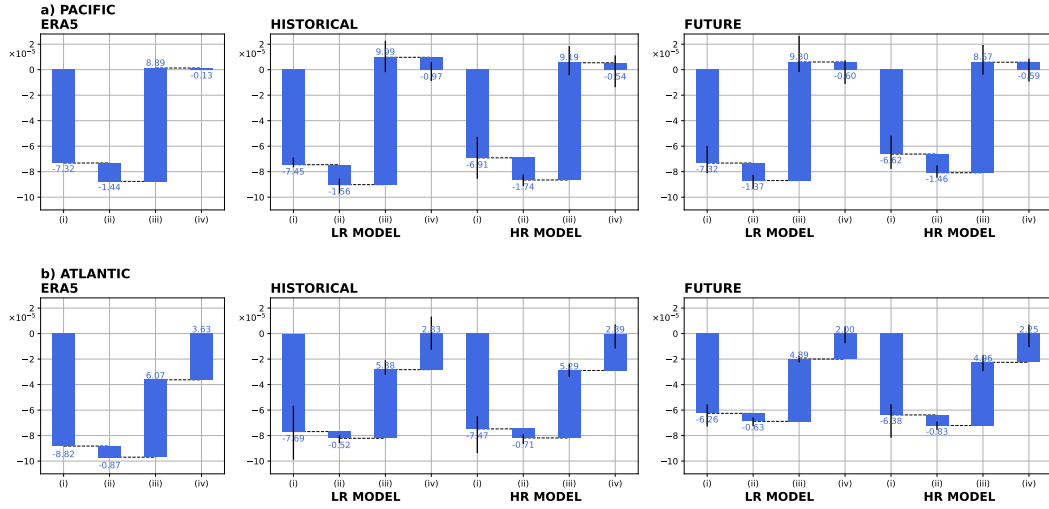
Figure 4. Waterfall chart of each term [m s^{-2}] in the LWA time tendency equation (Equation 3) separately plotted for a) Pacific and b) Atlantic sectors (encircled areas in Figure 2 and 3), computed with ERA5 (first column), historical runs for low-resolution and high-resolution models (middle column), and future runs (last column). Black bars indicate the value ranges across all the models used.

References

Athanasiadis, P. J., Ogawa, F., Omrani, N.-E., Keenlyside, N., Schiemann, R., Baker, A. J., . . . Gualdi, S. (2022, 11). Mitigating climate biases in the midlatitude North Atlantic by increasing model resolution: SST gradients and their relation to blocking and the jet. *Journal of Climate*, *35*, 6985-7006. Retrieved from `https://journals.ametsoc.org/view/journals/clim/35/21/JCLI-D-21-0515.1.xml` doi: 10.1175/JCLI-D-21-0515.1

Barnes, E. A. (2013). Revisiting the evidence linking Arctic amplification to extreme weather in midlatitudes. *Geophysical Research Letters*, *40*, 4734-4739. doi: 10.1002/grl.50880

Boville, B. A. (1991, may). Sensitivity of Simulated Climate to Model Resolution. *J. Clim.*, *4*(5), 469–485. Retrieved from `http://journals.ametsoc.org/doi/10.1175/1520-0442(1991)004{\%}3C0469:SOSCTM{\%}3E2.0.CO;2` doi: 10.1175/1520-0442(1991)004⟨0469:SOSCTM⟩2.0.CO;2

Cattiaux, J., Peings, Y., Saint-Martin, D., Trou-Kechout, N., & Vavrus, S. J. (2016). Sinuosity of midlatitude atmospheric flow in a warming world. *Geophysical Research Letters*, *43*, 8259-8268. doi: 10.1002/2016GL070309

Chen, G., Lu, J., Burrows, D. A., & Leung, L. R. (2015). Local Finite-Amplitude Wave Activity as an Objective Diagnostic of Midlatitude Extreme Weather. *Geophys. Res. Lett.*, *42*. doi: 10.1002/2015GL066959

Coumou, D., Lehmann, J., & Beckmann, J. (2015). The weakening summer circulation in the Northern Hemisphere mid-latitudes. *Science (80-.)*.(March), 1–8.

Davini, P., & D'Andrea, F. (2020). From CMIP3 to CMIP6: Northern Hemisphere atmospheric blocking simulation in present and future climate. *Journal of Climate*, *33*, 10021-10038. doi: 10.1175/JCLI-D-19-0862.1

Di Capua, G., & Coumou, D. (2016). Changes in meandering of the Northern Hemisphere circulation. *Environ. Res. Lett.*, *11*(9), 094028. Retrieved from `http://stacks.iop.org/1748-9326/11/i=9/a=094028?key=crossref.98f5b5d191331b0954b4bec87f0ee100` doi: 10.1088/1748-9326/11/9/094028

EC-Earth Consortium. (2018). *EC-Earth-Consortium EC-Earth3P-HR model output prepared for CMIP6 HighResMIP.* Earth System Grid Federation. doi: 10.22033/ESGF/CMIP6.2323

EC-Earth Consortium. (2019). *EC-Earth-Consortium EC-Earth3P model output prepared for CMIP6 HighResMIP hist-1950.* Earth System Grid Federation. doi: 10.22033/ESGF/CMIP6.4682

Francis, J. A., & Vavrus, S. J. (2012). Evidence linking Arctic amplification to extreme weather in mid-latitudes. *Geophysical Research Letters*, *39*, 1-6. doi: 10.1029/2012GL051000

Geen, R., Thomson, S. I., Screen, J. A., Blackport, R., Lewis, N. T., Mudhar, R., . . . Vallis, G. K. (2023, 11). An explanation for the metric dependence of the midlatitude jet-waviness change in response to polar warming. *Geophysical Research Letters*, *50*. doi: 10.1029/2023GL105132

Grams, C. M., & Archambault, H. M. (2016). The key role of diabatic outflow in amplifying the midlatitude flow: A representative case study of weather systems surrounding western North Pacific extratropical transition. *Monthly Weather Review*, *144*, 3847-3869. doi: 10.1175/MWR-D-15-0419.1

Haarsma, R. J., Roberts, M. J., Vidale, P. L., Catherine, A., Bellucci, A., Bao, Q.,

... Storch, J. S. V. (2016). High Resolution Model Intercomparison Project (HighResMIP v1.0) for CMIP6. *Geoscientific Model Development*, *9*, 4185-4208. doi: 10.5194/gmd-9-4185-2016

Hersbach, H., Bell, B., Berrisford, P., Hirahara, S., Horányi, A., Muñoz-Sabater, J., ... Thépaut, J. N. (2020). The ERA5 global reanalysis. *Quarterly Journal of the Royal Meteorological Society*, *146*, 1999-2049. doi: 10.1002/qj.3803

Huang, C. S. (2024, 1). *Python library: falwa (v1.2.1).* Retrieved from `https://github.com/csyhuang/hn2016_falwa` doi: 10.5281/zenodo.1234

Huang, C. S., & Nakamura, N. (2016). Local finite-amplitude wave activity as a diagnostic of anomalous weather events. *Journal of the Atmospheric Sciences*, *73*, 211-229. doi: 10.1175/JAS-D-15-0194.1

Huang, C. S., & Nakamura, N. (2017). Local wave activity budgets of the wintertime Northern Hemisphere: Implication for the Pacific and Atlantic storm tracks. *Geophysical Research Letters*, *44*, 5673-5682. doi: 10.1002/2017GL073760

Joos, H., Sprenger, M., Binder, H., Beyerle, U., & Wernli, H. (2023, 1). Warm conveyor belts in present-day and future climate simulations - part 1: Climatology and impacts. *Weather and Climate Dynamics*, *4*, 133-155. doi: 10.5194/wcd-4-133-2023

Madonna, E., Wernli, H., Joos, H., & Martius, O. (2014). Warm conveyor belts in the ERA-Interim dataset (1979-2010). Part I: Climatology and potential vorticity evolution. *Journal of Climate*, *27*, 3-26. doi: 10.1175/JCLI-D-12-00720.1

Martin, J. E. (2021). Recent Trends in the Waviness of the Northern Hemisphere Wintertime Polar and Subtropical Jets. *J. Geophys. Res. Atmos.*, *126*(9), 1–15. doi: 10.1029/2020JD033668

Martineau, P., Chen, G., & Burrows, D. A. (2017). Wave events: Climatology, trends, and relationship to Northern Hemisphere winter blocking and weather extremes. *Journal of Climate*, *30*, 5675-5697. doi: 10.1175/JCLI-D-16-0692.1

Nakamura, N., & Huang, C. S. (2018). Atmospheric blocking as a traffic jam in the jet stream. *Science*, *361*, 42-47. doi: 10.1126/science.aat0721

Nakamura, N., & Solomon, A. (2010, nov). Finite-Amplitude Wave Activity and Mean Flow Adjustments in the Atmospheric General Circulation. Part I: Quasigeostrophic Theory and Analysis. *J. Atmos. Sci.*, *68*(11), 2783–2799. doi: 10.1175/2011JAS3685.1

Neal, E., Huang, C. S. Y., & Nakamura, N. (2022, 4). The 2021 Pacific Northwest heat wave and associated blocking: Meteorology and the role of an upstream cyclone as a diabatic source of wave activity. *Geophysical Research Letters*, *49*. Retrieved from `https://onlinelibrary.wiley.com/doi/10.1029/2021GL097699` doi: 10.1029/2021GL097699

Nie, Y., Chen, G., Lu, J., Zhou, W., & Zhang, Y. (2023, 3). Constraining the varied response of Northern Hemisphere winter circulation waviness to climate change. *Geophysical Research Letters*, *50*. doi: 10.1029/2022GL102150

Pfahl, S., Schwierz, C., Grams, C. M., & Wernli, H. (2015). Importance of latent heat release in ascending air streams for atmospheric blocking. *Nature Geoscience*, *8*, 610-615. doi: 10.1038/NGEO2487

Roberts, C. D., Senan, R., Molteni, F., Boussetta, S., & Keeley, S. (2017a). *ECMWF ECMWF-IFS-HR model output prepared for CMIP6 HighResMIP.* Earth System Grid Federation. doi: 10.22033/ESGF/CMIP6.2461

Roberts, C. D., Senan, R., Molteni, F., Boussetta, S., & Keeley, S. (2017b). *ECMWF ECMWF-IFS-LR model output prepared for CMIP6 HighResMIP.* Earth System Grid Federation. doi: 10.22033/ESGF/CMIP6.2463

Roberts, C. D., Senan, R., Molteni, F., Boussetta, S., & Keeley, S. (2018). *ECMWF ECMWF-IFS-MR model output prepared for CMIP6 HighResMIP.* Earth System Grid Federation. doi: 10.22033/ESGF/CMIP6.2465

Röthlisberger, M., Pfahl, S., & Martius, O. (2016). Regional-scale jet waviness modulates the occurrence of midlatitude weather extremes. *Geophysical Research Letters*, *43*, 10,989-10,997. doi: 10.1002/2016GL070944

Scoccimarro, E., Bellucci, A., & Peano, D. (2017a). *CMCC CMCC-CM2-HR4 model output prepared for CMIP6 HighResMIP.* Earth System Grid Federation. doi: 10.22033/ESGF/CMIP6.1359

Scoccimarro, E., Bellucci, A., & Peano, D. (2017b). *CMCC CMCC-CM2-VHR4 model output prepared for CMIP6 HighResMIP.* Earth System Grid Federation. doi: 10.22033/ESGF/CMIP6.1367

Screen, J. A., & Simmonds, I. (2013). Exploring links between Arctic amplification and mid-latitude weather. *Geophys. Res. Lett.*, *40*(5), 959–964. doi: 10.1002/grl.50174

Tsujino, H., Urakawa, L. S., Griffies, S. M., Danabasoglu, G., Adcroft, A. J., Amaral, A. E., . . . Yu, Z. (2020, 8). Evaluation of global ocean-sea-ice model simulations based on the experimental protocols of the Ocean Model Intercomparison Project phase 2 (OMIP-2). *Geoscientific Model Development*, *13*, 3643-3708. doi: 10.5194/gmd-13-3643-2020

Tu, C.-Y. (2020a). *AS-RCEC HiRAM-SIT-HR model output prepared for CMIP6 HighResMIP.* Earth System Grid Federation. doi: 10.22033/ESGF/CMIP6.13301

Tu, C.-Y. (2020b). *AS-RCEC HiRAM-SIT-LR model output prepared for CMIP6 HighResMIP.* Earth System Grid Federation. doi: 10.22033/ESGF/CMIP6.13303

von Storch, J.-S., Putrasahan, D., Lohmann, K., Gutjahr, O., Jungclaus, J., Bittner, M., . . . Roeckner, E. (2017a). *MPI-M MPIESM1.2-HR model output prepared for CMIP6 HighResMIP.* Earth System Grid Federation. doi: 10.22033/ESGF/CMIP6.762

von Storch, J.-S., Putrasahan, D., Lohmann, K., Gutjahr, O., Jungclaus, J., Bittner, M., . . . Roeckner, E. (2017b). *MPI-M MPI-ESM1.2-XR model output prepared for CMIP6 HighResMIP.* Earth System Grid Federation. doi: 10.22033/ESGF/CMIP6.10290

Wang, M., Zhang, Y., & Lu, J. (2021, 5). The evolution dynamical processes of Ural blocking through the lens of local finite-amplitude wave activity budget analysis. *Geophysical Research Letters*, *48*. doi: 10.1029/2020GL091727

Woollings, T., Barriopedro, D., Methven, J., Son, S. W., Martius, O., Harvey, B., . . . Seneviratne, S. (2018). Blocking and its response to climate change. *Current Climate Change Reports*, *4*, 287-300. doi: 10.1007/s40641-018-0108-z

Yamamoto, A., Nonaka, M., Martineau, P., Yamazaki, A., Kwon, Y.-O., Nakamura, H., & Taguchi, B. (2021, 8). Oceanic moisture sources contributing to wintertime Euro-Atlantic blocking. *Weather and Climate Dynamics*, *2*, 819-840. Retrieved from `https://wcd.copernicus.org/articles/2/819/2021/` doi: 10.5194/wcd-2-819-2021